Materials Research. 2019; 22(3): e20180660
DOI: http://dx.doi.org/10.1590/1980-5373-MR-2018-0660

Fe_3O_4-TiO_2 and Fe_3O_4-SiO_2 Core-shell Powders Synthesized from Industrially Processed Magnetite (Fe_3O_4) Microparticles

***Virginia E. Noval*[a]*, *José G. Carriazo*[a]**

[a]*Estado Sólido y Catálisis Ambiental - ESCA, Departamento de Química, Facultad de Ciencias, Universidad Nacional de Colombia, Ciudad Universitaria, Bogotá, Colombia*

Received: October 06, 2018; Revised: February 09, 2019; Accepted: April 08, 2019

The interest for core-shells has been increased in the recent years due to their improved and modifiable properties. In this work, Fe_3O_4-TiO_2 and Fe_3O_4-SiO_2 core-shells were successfully synthesized from an industrially produced magnetite-rich powder with micro- and nanometric particle sizes, superparamagnetic behavior and saturation magnetization of 49 emu/g. The reverse microemulsion method was used to the synthesis of these core-shells. X-ray diffraction, energy dispersive X-ray analysis, electron microscopy (SEM-TEM), and magnetization curves were used to characterize the solids. Core-shells with different morphology and size, coating of crystalline TiO_2 (anatase) or amorphous silica, and superparamagnetic performance at room temperature (300 K) were obtained.

Keywords: *Core-shell, magnetite, magnetic powder, heterogeneous catalysis, catalytic support.*

1. Introduction

Core-shells are a relatively new family of particles. All micro- or nanoparticle constituted of either an internal particle (core) or a set of internal particles (multicore), and a simple or multiple coating material (shell) of different nature, is called a core-shell structure. A wide range of different structural combinations such as inorganic/inorganic, inorganic/organic, organic/inorganic, and organic/organic materials can be found in core-shell systems[1]. Core-shell structures often possess superb chemical and physical properties compared to their single-component counterparts[2]. Coating the particles with a thin shell of a compatible material makes it possible to control the inherent properties of powders, and introduces others desirable (physical and chemical) characteristics according to the nature of coating material, thereby improving their functional properties and expanding a broader range of potential application[3,4]. Core-shell structures are highly functional materials with modifiable surface properties, in some cases decreasing the sintering, increasing the surface area, reactivity and thermal stability, regarding single constituent materials[5,6]. Particularly, the applications of inorganic core-shell particles are found in many fields including biology, chemistry, physics and engineering[7], because of their multiple functions such as electrical, optical, magnetic, catalytic and electrocatalytic, among others[2,4,8,9,10].

Different morphologies of core-shell materials have been reported, such as spheres, wires, rods, tubes, belts, fibers, plates, sheets, cubes, etc.[2]. It is generally accepted that the performance of a catalyst can be strongly affected by its morphology, structure, and composition[10]. In heterogeneous catalysis, micro- or nanoparticles with high surface area are preferably used because generally more active catalysts are obtained as result of more dispersed and more exposed active phases. In order to reuse the catalysts and separate the products, solid particles have to be recovered after reaction by unit operations such as either centrifugation or filtration, but these procedures are difficult, impractical or simply inefficient when fine particles are used. For example, in environmental heterogeneous catalysis, recovering small particles from aqueous suspensions is very difficult, and these particles after used are frequently released into the aqueous effluents[11]. Several scientific works report that fine particles of TiO_2 can penetrate biological membranes of various microorganisms and plants, causing them death and provoking serious environmental damages in aqueous ecosystems[11,12]. Thus, there are several reasons to remove fine particles from reaction media after catalytic processes. The removal of fine particles from suspensions using magnetic fields is effective, and energetically more efficient and often faster than centrifugation or filtration[13]. In this sense, fine powders of heterogeneous catalysts designed with ferrimagnetic or superparamagnetic properties that allow their attraction by a magnetic field are enormously appreciated. Several types of core-shell systems have been synthesized using cores of magnetite (Fe_3O_4) and shells of different inorganic materials, to be used as heterogeneous catalysts or catalytic supports. Magnetite is a ferrimagnetic stable oxide[14], and thus the core-shell powders synthesized with this oxide are easily separated from liquid media by a magnetic field[4]. In recent years, magnetite has received great attention and has been enormously studied due to its attractive chemical and magnetic properties, low toxicity and its potential applicability in multidisciplinary fields such as catalysis, separation processes, biomedicine, biosensing,

*email: venovall@unal.edu.co

hyperthermia treatments, magnetic resonance imaging, and drug delivery[15-17].

Magnetite (Fe_3O_4) has been used as core in several core-shell systems with coating of silicon dioxide[18-20] or titanium dioxide[21,22], among others. These (Fe_3O_4-SiO_2 or Fe_3O_4-TiO_2) particulate systems are synthesized because of their enormous potential application as catalysts or catalytic supports, in which various linkers or specific chemical groups can be anchored in order to obtain magnetically separable catalysts. In addition, both silica and titania have low toxicity, protect the magnetite particles from thermal effects, chemical oxidation to hematite (a non-ferrimagnetic iron oxide), dissolution by acid attack, and agglomeration[18,20-22]. Titanium dioxide (TiO_2) is well recognized because of its photocatalytic activity and is widely used as photo-catalyst for degradation of organic pollutants in wastewater treatment.

Evidently, the scientific community has increased its endeavors on the synthesis of magnetite micro/nano-particles and the production of core-shell systems. In the literature, magnetite of high purity (synthesized in laboratories) is always used to synthesize the core-shell systems. However, the synthesis of magnetite is a crucial point for a possible real application of these systems. According to the literature, in all cases, magnetite for core-shell synthesis is prepared from diluted aqueous solutions of chemical reagents such as iron salts, e.g. $FeCl_3$ and $FeCl_2$, iron nitrates or sulfates, and bases such as ammonia or alkaline hydroxides[17,23-26]. On a large scale, this synthesis procedure will lead to environmental problems. In order to reduce economic costs and overcome the environmental impacts derived from this step, a new way of synthesis of core-shell systems has to be explored, in which industrially produced magnetite can be used. *Green Magnetita S.A.S.* is a Colombian company that produces industrial magnetite-rich powders for several uses. This micro-particulate material is industrially obtained from siderurgy wastes generated in iron-steel factories, by thermally assisted reduction processes in solid state, and without use of chemical reagents. This route involves green procedures with friendly outcomes for environment. From an economic point of view, currently 1 kg of this product has a price about USD 2.5, indicating a favorable value compared to the costs yielded from chemical procedures. In this paper, we report the synthesis of core-shell micro-particles from that (green magnetita®) product and making separate covering of both TiO_2 and SiO_2. The aim of this work is to advance on the synthesis procedure of these core-shell powders from an actually commercial, economic, green and industrially available magnetite-rich micro-particulate material. According to our knowledge, this is the first time that core-shell systems have been synthesized from industrially processed magnetite (Fe_3O_4) microparticles or nanoparticles.

2. Materials and Methods

2.1 Materials

Magnetite-rich powder was supplied by *Green Magnetita S.A.*S (Bogotá-Colombia). This industrial synthetic material was passed through a 325 ASTM mesh to obtain a fraction of particles lesser than 45 μm. The magnetic properties of this powder were preliminary checked using an ordinary magnet, observing that 100% of powder was attracted. Ammonium hydroxide (Merck, 28%), ethyl alcohol (Aldrich, 99.8%), acetone (Aldrich, 99.5%), cyclohexane (Merck, 99%), titanium(IV) butoxide (Aldrich, 97%), tetraethyl orthosilicate (Aldrich, 99%), and span 80 (sorbitan oleate, Merck) were used.

2.2 Synthesis of core-shell particles

Fe_3O_4-TiO_2 and Fe_3O_4-SiO_2 core-shell structures were synthesized using the reverse microemulsion method described in the literature[27-29] with some variations of the typical procedure. Here 10 mL of cyclohexane, 2 mL of Span 80 and 10 mg of commercial magnetite were mixed. This mixture was sonicated (equipment Branson 2510, 40 kHz) at room temperature for 10 minutes. Then, a volume of 0.8 mL of ammonium hydroxide (28%) was added to form the reverse microemulsion in which the microdrops of this solution are dispersed and stabilized by the polar fraction of Span 80 in cyclohexane phase. This microemulsion was subjected to mechanical stirring for 10 minutes in order to suspend the powder microparticles (magnetite) in the polar phase of the microemulsion. After that, a quantity (1.12 mL) of alkoxide (titanium butoxide or tetraethyl orthosilicate, according to the shell to be synthesized) was slowly added to the suspension under continuous stirring in an inert atmosphere, using a polyethylene glove-bag (Sigma-Aldrich, Z106089-1EA) saturated with nitrogen gas. The obtained mixture was left at rest, outer the bag, during 72 hours at room temperature (≈20 ºC). Finally, the solid fraction was separated by centrifugation (3000 rpm, 15 minutes) and purified by three washes with ethanol. The obtained solids were dried at room temperature for 8 hours, and then calcined at 400 ºC for 2 hours in static air atmosphere (a temperature ramp and heating rate of 10 ºC/min were used).

2.3 Characterization of solids

Chemical analysis of the magnetite-rich powder was carried out by X-ray fluorescence (XRF), using a Magix Pro PW-2440 Philips spectrometer with a rhodium tube and a maximum power of 4 kW. Before analysis, a sample of this material was dried at 100 ºC and then pressed at 120 kN on a spectrometric wax (Merck) to yield a standardized tablet of 36 mm diameter. Chemical analysis of the core-shell particles

was performed by energy dispersive X-ray analysis (EDX) from SEM exploration. Scanning electron microscopy (SEM) analyses were carried out with a microscope FEI Quanta 200, taking several images and EDX profiles at different points of the solids. The samples were previously metalized with a gold-palladium alloy using the sputtering technique (Quorum Q15OR ES metallizer). On the other hand, X-ray powder diffraction profiles were recorded using a Panalytical X'Pert PRO MPD equipment with copper anode (Cu Kα radiation: λ=1.54056 Å) and Bragg-Brentano configuration. All diffractograms were taken at room temperature, with 0.01º (2θ) step size and 10 s step time. Transmission electron micrographs (TEM analyses) were obtained using an electron microscope FEI TECNAI 20 Twin at 200 kV. The samples were previously dispersed in ethanol and analyzed on a copper grid covered with formvar resin.

Curie temperature of magnetite-rich powder was determined by thermogravimetric analysis (TGA) under a magnetic field. This measure was performed using 10 mg of sample in an alumina pan, a thermal analyzer TA Instruments SDT Q 600, nitrogen (N_2) atmosphere, and a magnet certified by TA Instruments, Inc. For this experiment, the magnet was put on the microbalance chamber in order to recording the changes of mass during a thermogravimetric analysis. The equipment was previously calibrated with high purity indium and sapphire. On the other hand, the magnetization curves of both magnetite-rich powder and core-shell solids were measured in a VersaLab Free 3 Tesla Cryogen-Free vibrating sample magnetometer, at 300 K, and between -30 and 30 kOe.

BET surface areas were determined from nitrogen adsorption isotherms. The isotherms were taken at 77 K using a Micromeritic ASAP 2020 adsorption analyzer in the P/P_0 range of 1×10^{-5} to 0.99. The samples were previously outgassed at 200 ºC for 8 h. On the other hand, acidity (Brönsted and Lewis) of the samples was qualitatively assessed by *in situ* diffuse reflectance infrared Fourier-transform spectroscopy (DRIFTS). The assessment was carried out using NH_3 as probe molecule, and an IR Tracer-100 (Shimadzu) FT-IR spectrometer with a Harrick Praying Mantis diffuse reflection spectroscopy accessory coupled to a high temperature reaction chamber[30]. According to a previous procedure described in the literature[30], each sample was preheated at 400 ºC in a flow of N_2 (10 mL/min) for 1 h. Then, after the sample was cooled (30 ºC), a stream (10 mL/min) of gas ammonia (5% in He) was passed through the sample for 15 min. After that, the sample was subjected to desorption for 30 min with a flow of N_2 (10 mL/min) at different temperatures (room temperature, 100 ºC, 200 ºC, 400 ºC). After this desorption at each indicated temperature, the IR spectra were *in situ* recorded at 30 ºC (150 scans with a resolution of 4 cm^{-1}). IR bands corresponding to N-H vibrations, when NH_3 is linked (coordinated) to acid sites, is used to observe the surface sites retaining ammonia[31]. Brönsted acidity[31] is observed about 1435 cm^{-1}, and Lewis acidity[31] around 1600 cm^{-1}. Prior to ammonia adsorption, a background spectrum was acquired for bare (clean) sample in order to compare the IR bands.

3. Results and Discussion

3.1 Characterization of industrial magnetite-rich powder

Chemical analysis (Table 1) reveals the high content of iron (97.666% reported as Fe_3O_4) in the magnetite-rich powder, indicating a probable high content of magnetite. However, small quantities of other elements such as Si, Mn, Ti and Cu were observed. These elements are contaminants coming from the industrially processed siderurgy wastes. Likewise, EDX analysis (Figure 1a) reveals iron species as the main constituents and small contents of other elements in the surface. SEM and TEM micrographs (Figures 1b and 1c) show varied morphology and size of particles in this powdered material, including nanoscale and microscale levels.

The X-ray diffraction analysis of magnetite-rich powder (Figure 2) revealed that magnetite is the principal component of this material, with other phases of iron oxides, hematite (α-Fe_2O_3) and wustite (FeO). All peaks were identified according to the literature[32-34]. The peaks at 2θ (º) = 18.4, 30.1, 35.5, 37.2, 43.2, 53.5, 57.0, 62.6, and 74.0 are assigned to magnetite (Fe_3O_4). All the XRD signals are indexed in Table 2, including the $d_{(hkl)}$ interplanar spacing values, and the corresponding peaks are labeled in Figure 2. On the basis of the crystalline structures identified by XRD, a semiquantitative estimation of these phases leads to the following approximation: 68% of Fe_3O_4, 8% α-Fe_2O_3 and 24% of FeO. Although other iron oxides different to magnetite are contained in this powder, it is possible to consider that these phases are intimately integrated because all of the powder (100% of the grains) is attracted by a regular magnet.

Table 1. Chemical analysis of the magnetite-rich powder.

Element analyzed (some values expressed as oxides)	Content (wt.%)as
Fe_3O_4	97.666
SiO_2	0.845
Mn	0.820
Al_2O_3	0.134
Cu	0.140
SO_3	0.116
Cr	0.103
CaO	0.076
P_2O_5	0.035
MgO	0.030
Ti	0.012
V	0.012
Mo	0.011

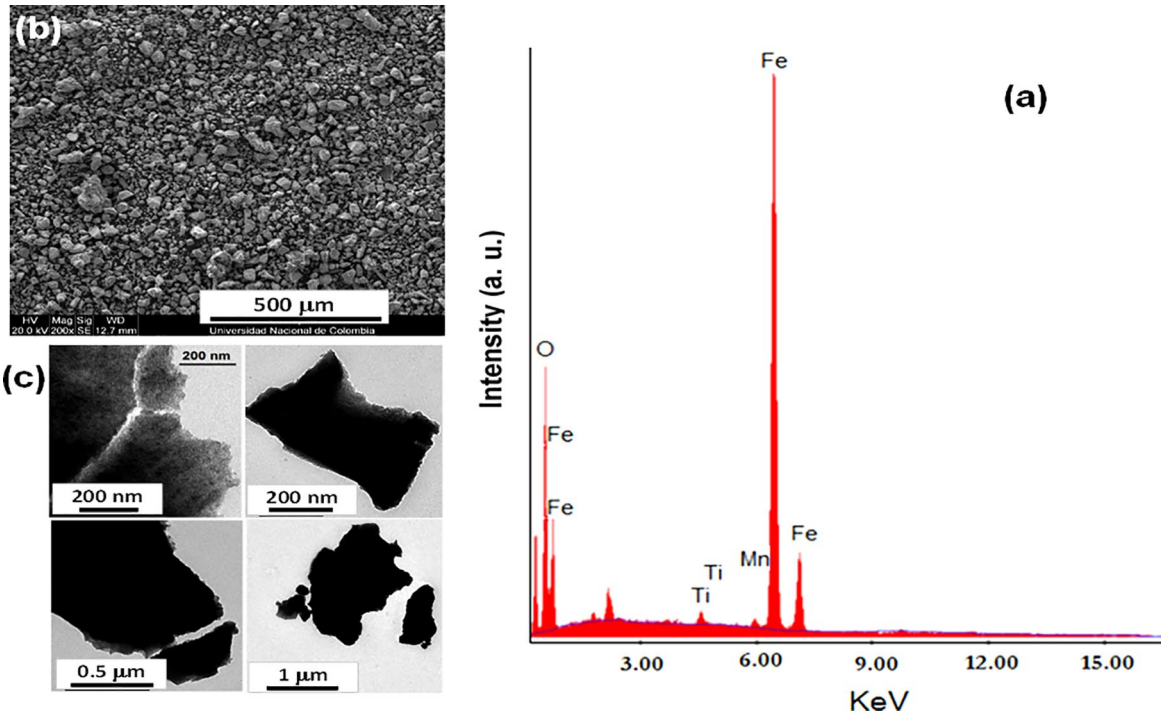

Figure 1. EDX analysis **(a)** and electron micrographs, SEM **(b)** and TEM **(c)**, of magnetite-rich powder.

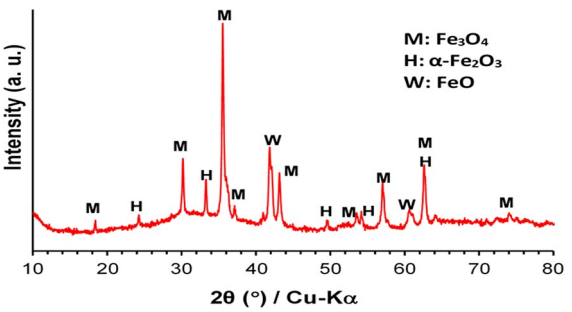

Figure 2. X-ray diffraction profile of the (industrially obtained) magnetite-rich powder. **M**: magnetite (Fe_3O_4), **H**: hematite (α-Fe_2O_3), and **W**: wustite (FeO).

Table 2. X-ray diffraction positions (2θ) and the interplanar spacing values (d_{hkl}) of different iron oxides phases found in the magnetite-rich powder.

2θ (º)	d (Å)	(hkl)	Phase (microstructure)
18.4	4.81	(111)	Magnetite (Fe_3O_4)
24.2	3.67	(012)	α-Fe_2O_3
30.1	2.96	(220)	Magnetite (Fe_3O_4)
33.2	2.70	(104)	α-Fe_2O_3
35.5	2.52	(311)	Magnetite (Fe_3O_4)
37.2	2.41	(222)	Magnetite (Fe_3O_4)
41.8	2.16	(200)	FeO (wustite)
43.2	2.09	(400)	Magnetite (Fe_3O_4)
49.6	1.84	(024)	α-Fe_2O_3
53.5	1.71	(422)	Magnetite (Fe_3O_4)
54.1	1.69	(116)	α-Fe_2O_3
57.0	1.61	(511)	Magnetite (Fe_3O_4)
60.6	1.52	(220)	FeO (wustite)
62.6	1.48	(440), (214)	Magnetite + α-Fe_2O_3
74.0	1.28	(533)	Magnetite (Fe_3O_4)

The Magnetization-demagnetization of magnetite-rich powder (Figure 3a) displays the superparamagnetic character of this material, since the magnetization curve does not show a hysteresis loop[35,36], thus a very low coercive force (approximately zero) is obtained. Bulk magnetite is typically a ferrimagnetic material with both saturation magnetization (85-100 emu/g) and coercivity higher than those of Fe_3O_4 fine powders[35,37], but the superparamagnetic behavior of this material is a result of small particle sizes in fine powder (micro to nanoparticles). A superparamagnet is defined as an assembly of non-interacting giant magnetic moments[36], which is frequently encountered in magnetite fine powders. This magnetic behavior of very low coercive force is actually interesting because no remaining magnetization is obtained when a magnetic field is retired, which avoids the particle agglomeration. Thus, it is important to stand out that the largest magnetite nanoparticles that still show superparamagnetic properties are the best to be used in adsorption and catalysis systems[26]. A saturation magnetization of 49 emu/g was measured, which is in the range of values (30 to 80 emu/g) reported in the literature (at 300 K) for synthetic magnetite fine powders[23,36,38]. The saturation magnetization is influenced by particle size, morphology, shape anisotropy[37], and impurities in the sample. On the other

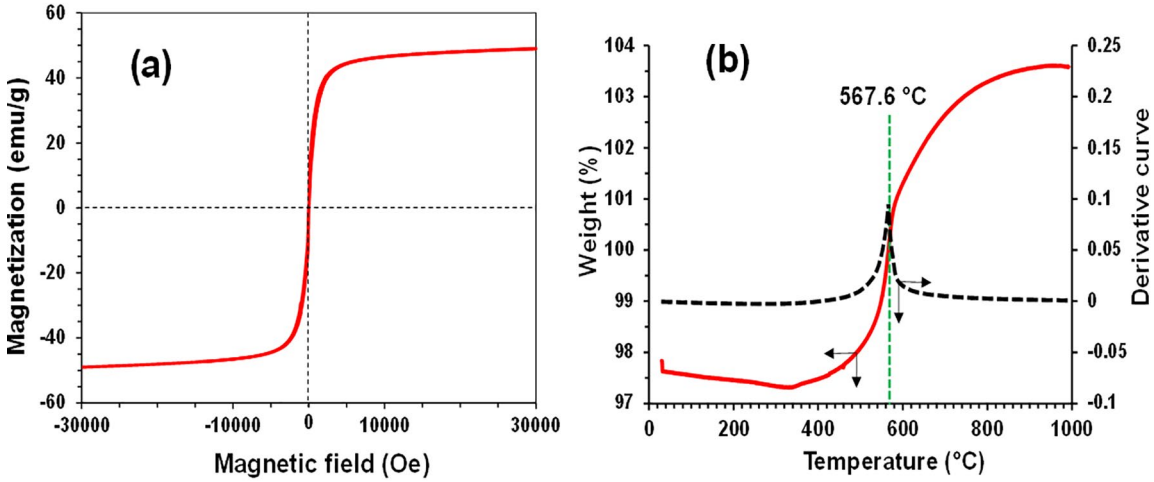

Figure 3. Magnetization curve at 300 K **(a)** and Curie temperature determination by TGA (using N_2 atmosphere) under a magnetic field **(b)** for the magnetite-rich powder.

hand, Figure 3b shows the Curie temperature (567.6 ºC) determined by TGA under a magnetic field. At temperature values higher than 567.6 ºC this magnetite-rich powder loses its magnetic properties and is not attracted by the magnetic field put above, thus an abrupt gain of mass is registered by the microbalance. According to the literature, Curie temperature is around 584 ºC[39,40], although other works have reported 577 ºC[38], 565 ºC[41] and 440 ºC[42] depending on the synthesis procedures and structural and morphological variations. Curie temperature is a very important parameter because several (magnetic) applications at high temperature may be restricted. At this value of temperature, a ferromagnetic, ferrimagnetic or superparamagnetic solid changes to be merely a paramagnetic material.

3.2 Magnetic core-shell structures

Taking into account the good magnetic properties of the magnetite-rich powder, this industrial product was used as core in the synthesis of Fe_3O_4-TiO_2 and Fe_3O_4-SiO_2 core-shell powders by using the reverse microemulsion method. Efficiency of the synthesis was determined as 76.3% for Fe_3O_4-TiO_2 and 86.2 for Fe_3O_4-SiO_2. The TiO_2 and SiO_2 contents were also stoichiometrically calculated. The content of TiO_2 in Fe_3O_4-TiO_2 core-shells is 20.0 wt.%, whereas the SiO_2 content in Fe_3O_4-SiO_2 core-shells is 22.9 wt.%. Because the densities of TiO_2 and SiO_2 (powders) are considerably lower than that of magnetite, the percentages of titania and silica incorporated in the solids represent an important covering volume (shell). At this point, it is important to mention that a comparison with literature results is very difficult because the percentages of silica and titania incorporated in the core-shells are not frequently indicated. Instead of that, the literature reports the thickness of shells. The morphology (SEM analysis) of microparticles obtained by coating magnetite-rich powder with TiO_2 is observed in Figure 4. Rugose particles with irregular morphology (like raisins) and size about 100 (m, and less than that, were observed by SEM. Energy dispersive X-ray analysis (EDX) revealed the high content of titanium in the shell of particles with no signal of iron on the most of these particles. However, for some particles, a small signal of iron was detected as consequence of an irregular coating (Figure 4). Non-spherical morphology for the Fe_3O_4-TiO_2 system is probably a result of the high reactivity of titanium alkoxide in aqueous (ammonia solution) micromicelles formed by the reverse microemulsion method. Titanium alkoxides are more reactive than silicon or aluminum alkoxides. The very fast hydrolysis of titanium alkoxide (titanium tetrabutoxide) led to rugose surface coating. In addition, TEM images (Figure 5) reveal nanometric domains with nanoparticles agglomeration. Irregular morphology is again identified at nanometric scale, confirming the formation of nanoparticles of Fe_3O_4-TiO_2 with core-shell structures.

On the other hand, the synthesis of Fe_3O_4-SiO_2 led to the formation of perfectly spherical microparticles (Figure 6) below 50 (m in size. The more regular and homogeneous covering of this core-shell system perhaps is consequence of the lower reactivity of the silicon alkoxide (silicon tetraethoxide), in the aqueous micromicelles, regarding that of titanium alkoxides. According to the literature, the hydrolysis rate constant for a $Ti(OR)_4$ ($k_h = 10^{-3}$ M^{-1} S^{-1}) is more than five order of magnitude greater than that of $Si(OEt)_4$ ($k_h = 5x10^{-9}$ M^{-1} S^{-1}) at pH 7[43]. The lower hydrolysis rate for silicon alkoxides allows building well distributed microshell structures around the cores, yielding core-shell microparticles with homogeneous surface. The EDX analyses on the Fe_3O_4-SiO_2 particles (Figure 6) revealed the high content of silicon in the shell of particles with no signal of iron for any particle, which indicates that iron oxide is completely

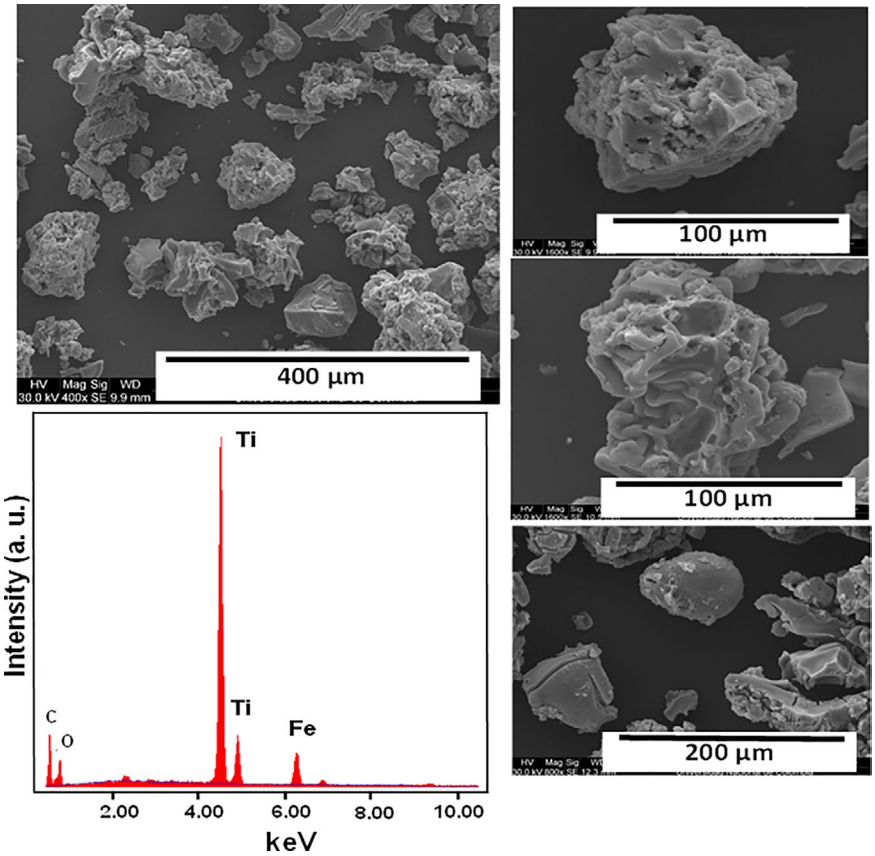

Figure 4. Scanning electron micrographs (SEM images) and EDX analysis of the Fe_3O_4-TiO_2 core-shell system.

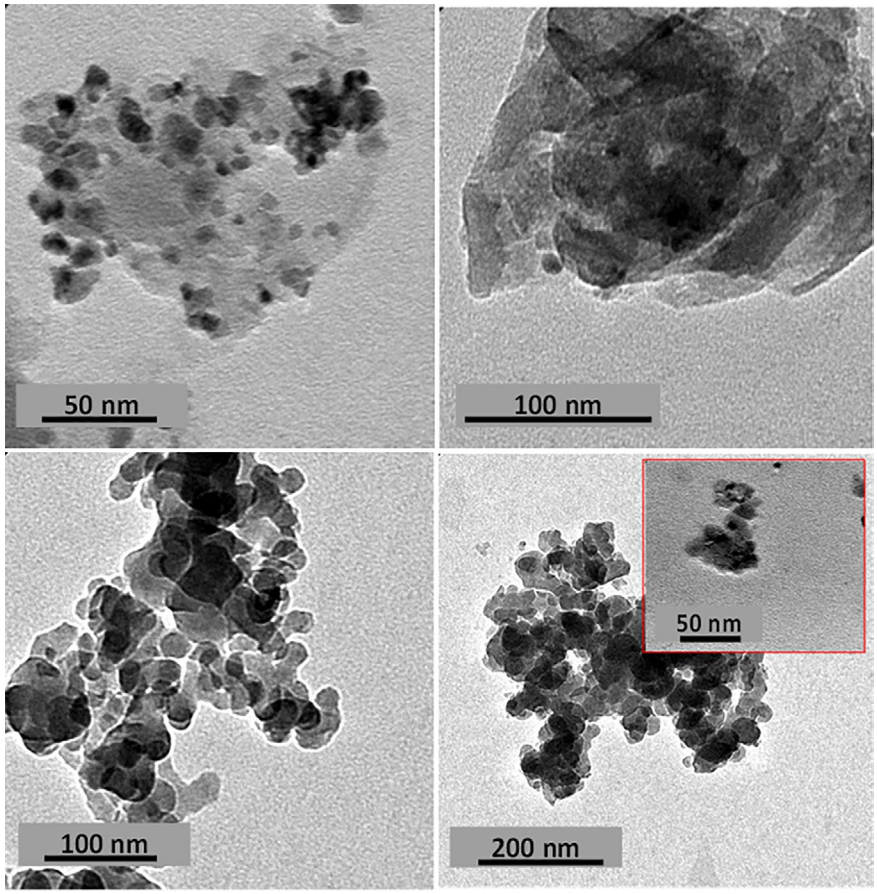

Figure 5. Transmission electron micrographs (TEM images) of the Fe_3O_4-TiO_2 core-shell system.

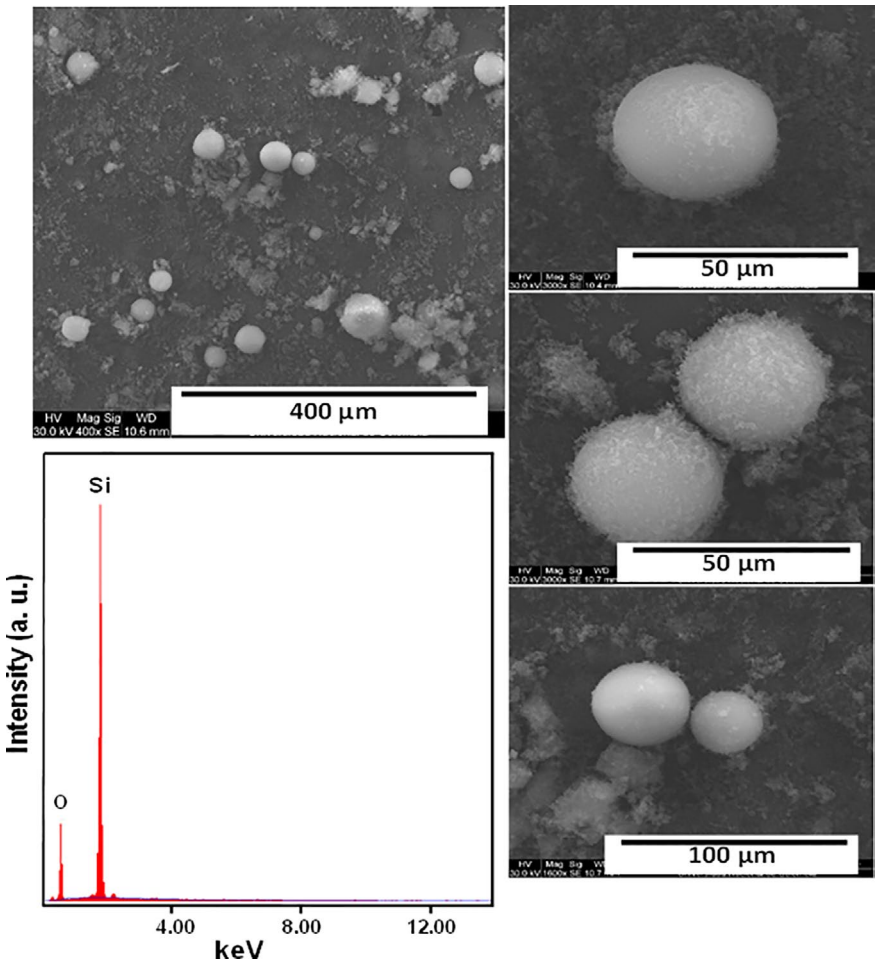

Figure 6. Scanning electron micrographs (SEM images) and EDX analysis of the Fe_3O_4-SiO_2 core-shell system.

hidden. Additionally, TEM images (Figure 7) confirm the formation of spherical and discrete nanoparticles with size less than 150 nm. This result ratifies the suitable formation of both micro and nanometric Fe_3O_4-SiO_2 core-shells from magnetite-rich powder and the reverse microemulsion method.

The magnetization curves at 300 K for the Fe_3O_4-TiO_2 and Fe_3O_4-SiO_2 core-shell particles (Figure 8) confirm the superparamagnetic performance of these materials, since no hysteresis loop (zero coercive force) can be observed[28,35,44]. This behavior is coherent and is a result derived from the magnetic properties of magnetite-rich material introduced as cores in the particles. The saturation magnetization values of Fe_3O_4-TiO_2 and Fe_3O_4-SiO_2 (1.37 emu/g and 1.40 emu/g, respectively) are significantly lower than that showed for magnetite-rich powder, which is consequence of the covering (shell) with non-magnetic materials (TiO_2 or SiO_2). However, these saturation magnetization values are sufficient to give a suitable response under a moderate magnetic field, allowing well separation of particles from liquid media, such as it was experimentally observed (Figure 8). Recent studies have demonstrated that the saturation magnetization of silica-coated Fe_3O_4 nanoparticles decreases up to 1.9 emu/g as the silica shell thickness increases to 18.5 nm[28]. Zhang and Wang[44] reported a strong decrease from 70 to 8 emu/g in magnetite coated with carbon shells, and Yang et al.[35] observed a reduction from 56 to 1.4 emu/g as result of coating Fe_3O_4 with SiO_2. Extending this conclusion to the present work, a well coating for the iron oxide is expected in both core-shells Fe_3O_4-TiO_2 and Fe_3O_4-SiO_2.

X-ray diffraction (XRD) analysis of the Fe_3O_4-TiO_2 powder reveals the characteristic signals of (TiO_2) anatase phase (Figure 9). The peaks at 2-theta positions (º) of 25.2, 37.9, 48.0, 54.4, 62.6. 70.0 and 75.5 clearly confirm the successful formation of a TiO_2 shell (anatase phase) on the iron oxide. All of these diffraction peaks were confirmed by literature[21,22,45]. On the other hand, the Fe_3O_4-SiO_2 powder shows an XRD amorphous profile (Figure 9) with a broad signal about $2\theta = 23º$ (between 15 and 30º). This is a typical profile of silica (SiO_2), and confirms the successful formation of SiO_2 shell on the magnetite-rich particles. In both XRD profiles, very small signals of the highest magnetite peaks (2θ = 35.5 and 62.6º) were observed. Similar results have

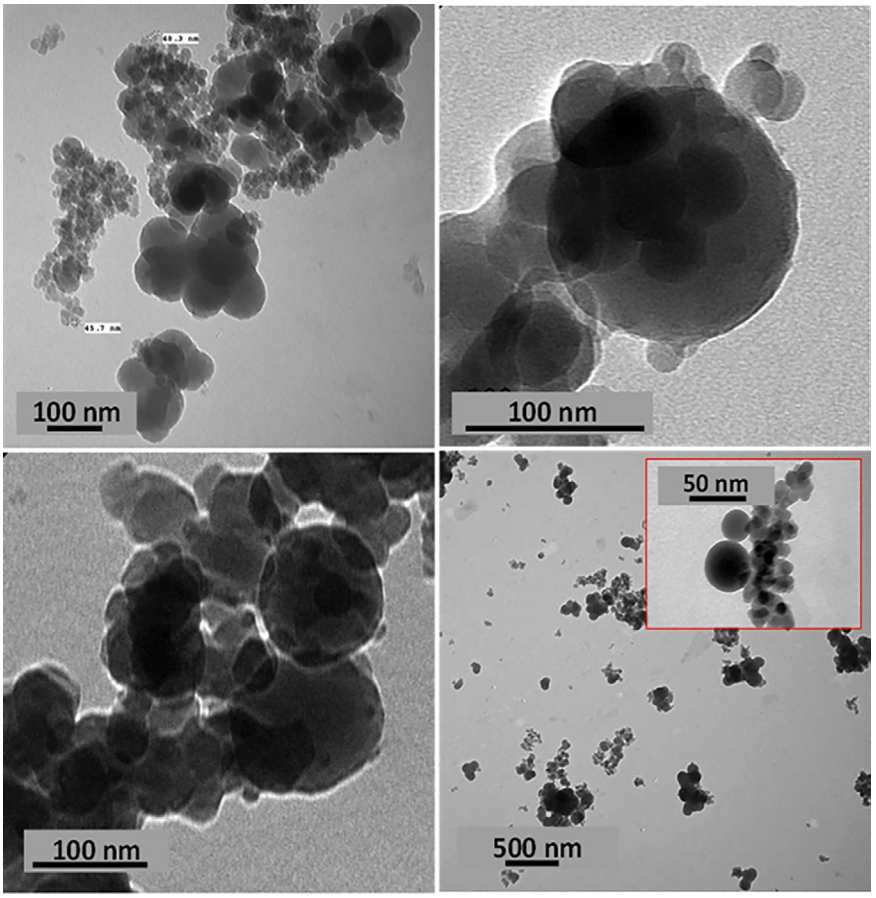

Figure 7. Transmission electron micrographs (TEM images) of the Fe_3O_4-SiO_2 core-shell system.

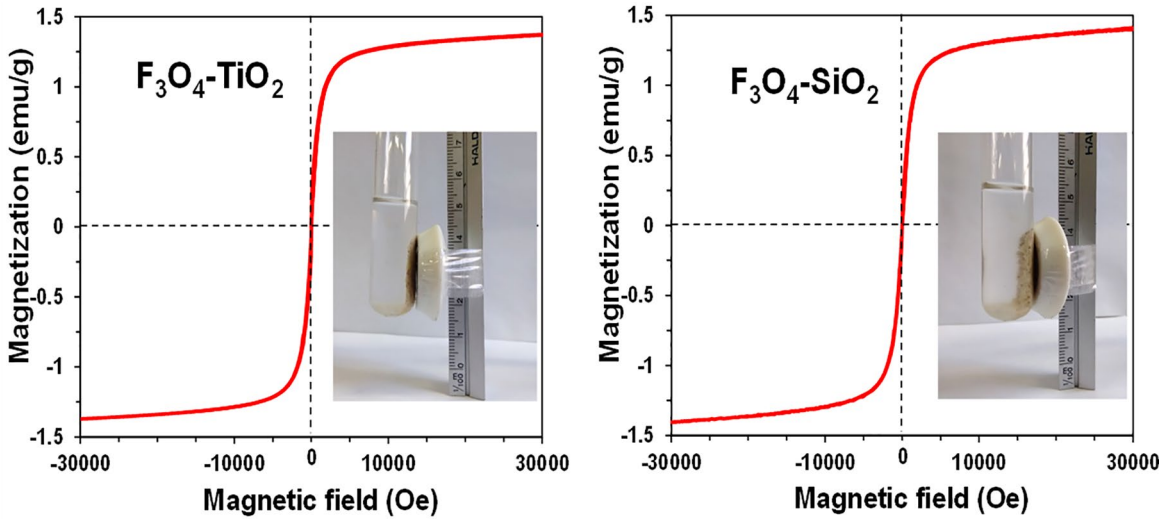

Figure 8. Magnetization curves, at 300 K, for Fe_3O_4-TiO_2 and Fe_3O_4-SiO_2 core-shell systems. The inserts show the attraction of these powders in water using a magnet.

been obtained by other researchers for Fe_3O_4-SiO_2 core-shells[20,28] and Fe_3O_4-TiO_2 core shells[21,46] using pure magnetite synthesized in laboratories. XRD signals corresponding to magnetite (core of the systems) are difficult to be observed because a good covering of TiO_2 or SiO_2 was formed. It is well known that the shielding or absorption effects by coating structures lead to the weakening of the XRD intensities coming from the reflections of cores[22,46]. Core-shell formation is verified because these particulate systems have superparamagnetic behavior, and a magnet equally attracts

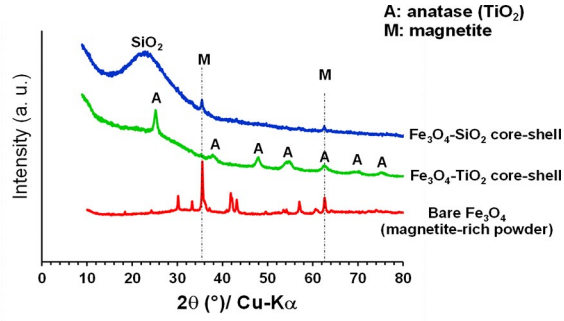

Figure 9. X-ray diffraction profiles of the Fe_3O_4-TiO_2 and Fe_3O_4-SiO_2 core-shell systems and their comparison with the industrial magnetite-rich powder.

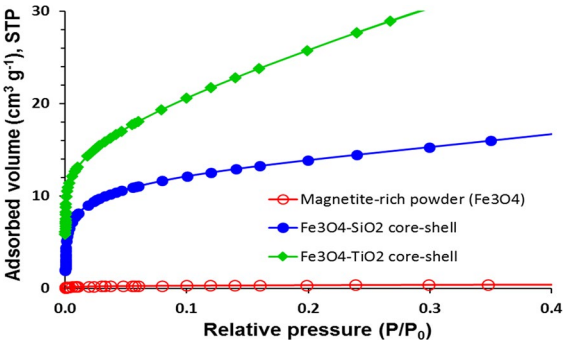

Figure 10. Nitrogen adsorption isotherms at 77K obtained for the magnetite-rich powder and core-shells (Fe_3O_4-TiO_2 and Fe_3O_4-SiO_2).

all the particles. The reason whereby these titania-rich or silica-rich particles are attracted under a magnetic field is that they have magnetite cores.

All the basic aforementioned characterizations confirm the effectiveness of the reverse microemulsion method to suspend relatively large particles (microparticles) of a dense materials such as magnetite. One of the difficulties found in previous assays focused to extend the magnetite core-shell synthesis to practical situations has been the suspension of large particles, so the synthesis of magnetite for this purpose is usually restricted to obtain nanoparticles. The present study demonstrates that the reverse microemulsion method is suitable for overcoming this drawback.

On the other hand, the N_2 adsorption isotherms of magnetite-rich powder and core-shells (Figure 10) give valuable information about the surface and porosity of these solids. Clearly, magnetite-rich powder is a non-porous material due to its negligible N_2-adsorption level, whereas the Fe_3O_4-TiO_2 and Fe_3O_4-SiO_2 core-shells increased the porosity and as consequence of that they significantly improved their adsorption capacity. BET surface area of magnetite-rich powder (Fe_3O_4) is insignificant (1 m^2/g), but increased to 95 m^2/g and 46 m^2/g for Fe_3O_4-TiO_2 and Fe_3O_4-SiO_2, respectively. This result indicates that covering magnetite with TiO_2 or SiO_2 is very important to yield large surface areas. Thus, the core-shell systems obtained in the present work are magnetic solids with potential value to be used as catalysts or catalytic supports. The higher surface area value for Fe_3O_4-TiO_2 core-shell is directly related to the higher roughness of the particles, which was verified by SEM. These BET surface areas are comparable with those obtained by other authors for these core-shell systems. Costa and coworkers[47] reported 141 m^2/g for Fe_3O_4-SiO_2-TiO_2 (a core-shell-shell system) and Zhang et al.[21] reported 40 m^2/g for Fe_3O_4-C-TiO_2, whereas Lee et al.[48] synthesized Fe_3O_4-SiO_2 core-shells with BET surface area of 41 m^2/g.

In situ DRIFTS analyses of NH_3 adsorbed and desorbed at different temperatures revealed acidity generation (Brönsted and Lewis sites) after covering of magnetite-rich powder with TiO_2 or SiO_2. DRIFTS spectra of the solids with ammonia adsorbed at room temperature and after heating at 100 ºC, 200 ºC and 400 ºC are showed in Figure 11. It is clear that magnetite-rich powder does not adsorb ammonia (Figure 11a), indicating that it does not have acid sites. However, DRIFTS spectra of both Fe_3O_4-TiO_2 and Fe_3O_4-SiO_2 core-shells (Figures 11b-c) clearly show a broad band between 3000 and 3500 cm^{-1}, which is attributed to the NH_3 adsorbed to acid sites[49-51]. This band is reduced according to the heating, as consequence of releasing chemisorbed NH_3 from the solids. The bands about 1600 cm^{-1} and 1435 cm^{-1} are typically assigned to vibrations of NH3 retained on Lewis and Brönsted acid sites[30,31,50]. These bands also decrease during heating, in response to the acid strength of the sites. From the spectra of Fe_3O_4-SiO_2 it is evident that the intensity of all the bands is strongly reduced after heating at 100 ºC, which allows concluding that this solid has acid sites weaker than Fe_3O_4-TiO_2.

4. Conclusions

Fe_3O_4-TiO_2 and Fe_3O_4-SiO_2 core-shell particles were successfully synthesized from a commercial and industrially produced magnetite-rich powder. Industrial fine powder was carefully characterized revealing the predominant composition and behavior of magnetite having a wide range of particle size (from micrometers to nanometers) and superparamagnetic performance (no coercivity, saturation magnetization of 49 emu/g and Curie temperature of 567.6 ºC). The core-shell systems were synthesized by using the reverse microemulsion method. SEM, TEM, XRD and magnetization curves confirm the formation of superparamgnetic core-shells (no coercivity, and saturation magnetization around 1.4 emu/g) at level of micro and nanoparticles, with coating of TiO_2 (anatase phase) and SiO_2 (amorphous silica). In addition, all these results confirm the appropriate performance of coating method (reverse microemulsion) used here for the core-shell synthesis, demonstrating its efficiency to suspend microparticles with large size of dense materials such as magnetite. The formation of a microemulsion with large size particles of magnetite, more than nanoparticles, is also a challenge for real industrial process. The covering of magnetite-rich powder with TiO_2

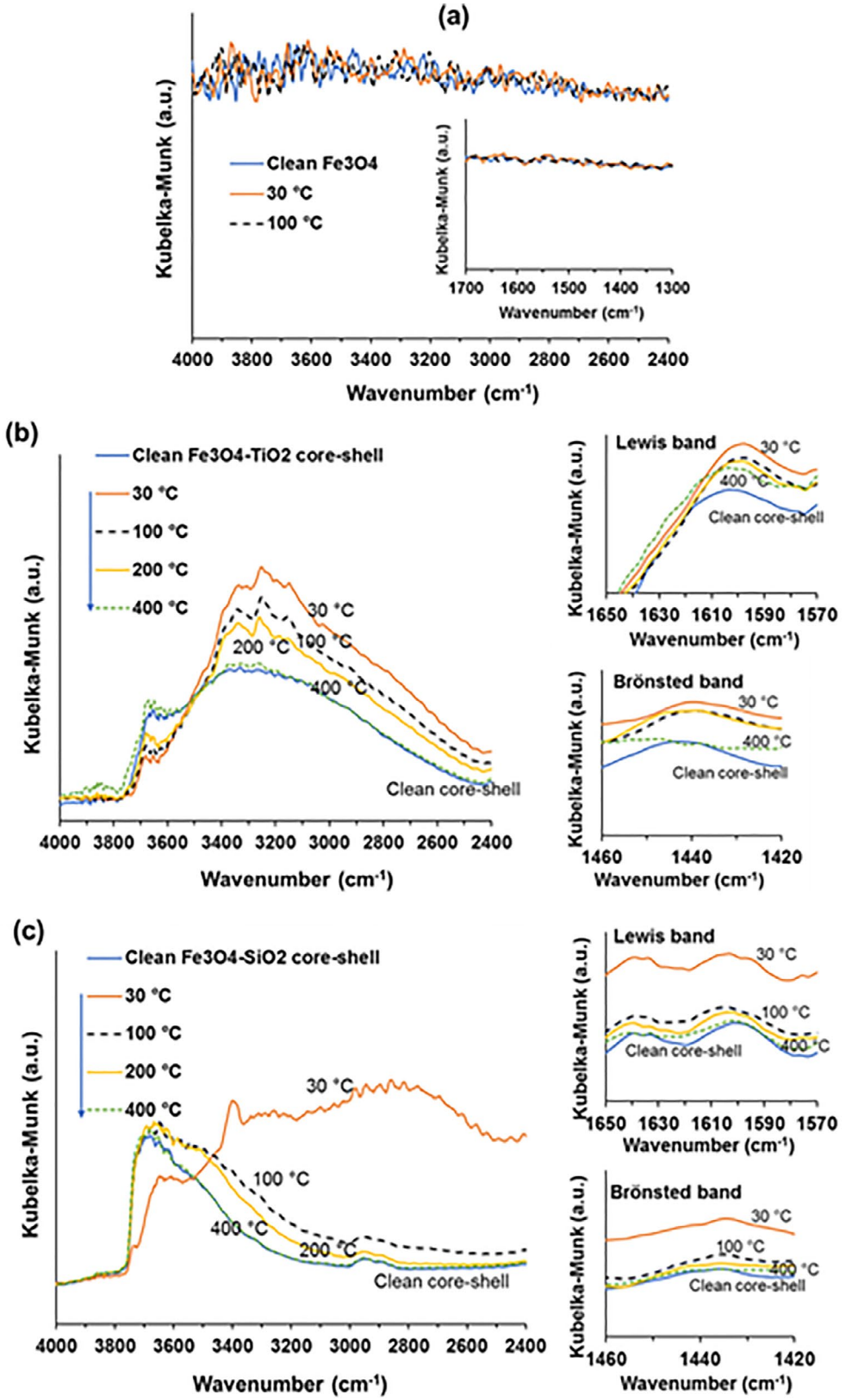

Figure 11. *In situ* DRIFTS spectra of NH_3 adsorbed on the solids at different temperatures. **a)** Magnetite-rich powder (Fe_3O_4), **b)** Fe_3O_4-TiO_2 core-shell, and **c)** Fe_3O_4-SiO_2 core-shell. Brönsted and Lewis acidity bands are observed about 1435 cm^{-1} and 1600 cm^{-1}, respectively.

and SiO_2 led to the formation magnetic core-shell systems with important surface area values and acidity.

5. Acknowledgements

The authors gratefully acknowledge the (U. N.) Universidad Nacional de Colombia (Bogotá, D.C.). This work was developed at the 125-Lab (Lab-DRES: Laboratorio de Diseño y Reactividad de Estructuras Sólidas) of the Faculty of Science (U.N.-Bogotá). The authors also thank the company *Green Magnetita S.A.*S (Bogotá-Colombia) for providing the industrial magnetite samples.

6. References

1. Chaudhuri R, Paria S. Core/Shell Nanoparticles: Classes, Properties, Synthesis Mechanisms, Characterization, and Applications. *Chemical Reviews*. 2012;112(4):2373-2433.
2. Lu W, Guo X, Luo Y, Li Q, Zhu R, Pang H. Core-shell materials for advanced batteries. *Chemical Engineering Journal*. 2019;355:208-237.
3. Liu G, Hong G, Sun G. Synthesis and characterization of SiO_2/Gd_2O_3:Eu core-shell luminescent materials. *Journal of Colloid and Interface Science*. 2004;278(1):133-138.
4. Li W, Elzatahry A, Aldhayan D, Zhao D. Core-shell structured titanium dioxide nanomaterials for solar energy utilization. *Chemical Society Reviews*. 2018;47(22):8203-8237.
5. Zhang Q, Lee I, Joo JB, Zaera F, Yin Y. Core-Shell Nanostructured Catalysts. *Accounts of Chemical Research*. 2013;46(8):1816-1824.
6. Zhang N, Liu S, Xu YJ. Recent progress on metal core@ semiconductor shell nanocomposites as a promising type of photocatalyst. *Nanoscale*. 2012;4(7):2227-2238.
7. Mélinon P, Begin-Colin S, Duvail JC, Gauffre F, Boime NH, Ledoux G, et al. Engineered inorganic core/shell nanoparticles. *Physics Reports*. 2014;543(3):163-197.
8. Yang S, Tan Y, Yin X, Wang L, Wang H, Zhou Y. A facile and green approach to prepare monodispersion nanonickel nanofluids. *Particulate Science and Technology*. 2018;36(2):141-145.
9. Han T, Peng L, Cao S, Zhu D, Tu M, Zhang J. Preparation of a Core-Shell Structured Al2O3/YAG:Ce Phosphor by a Spray Drying Method and Formation Mechanism. *Rare Metal Materials and Engineering*. 2014;43(10):2311-2315.
10. Jiang R, Tung S, Tang Z, Li L, Ding L, Xi X, et al. A review of core-shell nanostructured electrocatalysts for oxygen reduction reaction. *Energy Storage Materials*. 2018;12:260-276.
11. Torres-Luna JA, Carriazo JG, Sanabria NR. Delaminated montmorillonite with iron(III)-TiO_2 species as a photocatalyst for removal of a textile azo-dye from aqueous solution. *Environmental Technology*. 2016;37(11):1346-1356.
12. Ma H, Brennan A, Diamond S. Phototoxicity of TiO_2 nanoparticles under solar radiation to two aquatic species: Daphnia magna and Japanese Medaka. *Environmental, Toxicology and Chemistry*. 2012;31(7):1621-1629.
13. Tang H, Yu CH, Oduoro W, He H, Tsang SC. Engineering of a Monodisperse Core-Shell Magnetic Ti-O-Si Oxidation Nanocatalyst. *Langmuir*. 2008;24(5):1587-1590.
14. Parkinson GS. Iron oxide surfaces. *Surface Science Reports*. 2016;71(1):272-365.
15. Fodjo EK, Gabriel KM, Serge BY, Li D, Kong C, Trokourey A. Selective synthesis of $Fe_3O_4Au_xAg_y$ nanomaterials and their potential applications in catalysis and nanomedicine. *Chemistry Central Journal*. 2017;11:58.
16. Carriazo Baños JG, Noval Lara VE, Ochoa-Puentes C. Magnetite (Fe_3O_4): An inorganic structure with many applications for heterogeneous catalysis. *Revista Colombiana de Química*. 2017;46(1):42-59.
17. Baeza A, Guillena G, Ramón DJ. Magnetite and Metal-impregnated Magnetite Catalysts in Organic Synthesis: A Very Old Concept with New Promising Perspectives. *ChemCatChem*. 2016;8(1):49-67.
18. Cendrowski K, Sikora P, Zielinska B, Horszczaruk E, Mijowska E. Chemical and thermal stability of core-shelled magnetite nanoparticles and solid silica. *Applied Surface Science*. 2017;407:391-397.
19. Lu CH, Chen GH, Yu B, Cong HL, Kong LM, Guo L. Design and synthesis of Fe_3O_4@SiO_2 core-shell nanomaterials. *Integrated Ferroelectrics*. 2017;182(1):46-52.
20. Wang S, Tang J, Zhao H, Wan J, Chen K. Synthesis of magnetite-silica core-shell nanoparticles via direct silicon oxidation. *Journal of Colloid and Interface Science*. 2014;432:43-46.
21. Zhang Q, Meng G, Wu J, Li D, Liu Z. Study on enhanced photocatalytic activity of magnetically recoverable Fe3O4@C@ TiO2 nanocomposites with core-shell nanostructure. *Optical Materials*. 2015;46:52-58.
22. Zheng J, Wu Y, Zhang Q, Li Y, Wang C, Zhou Y. Direct liquid phase deposition fabrication of waxberry-like magnetic Fe_3O_4@ TiO_2 core-shell microspheres. *Materials Chemistry and Physics*. 2016;181:391-396.
23. Kumar R, Sakthivel R, Behura R, Mishra BK, Das D. Synthesis of magnetite nanoparticles from mineral waste. *Journal of Alloys and Compounds*. 2015;645:398-404.
24. Chinnaraj K, Manikandan A, Ramu P, Arul Antony S, Neeraja P. Comparative Studies of Microwave- and Sol-Gel-Assisted Combustion Methods of Fe_3O_4 Nanostructures: Structural, Morphological, Optical, Magnetic, and Catalytic Properties. *Journal of Superconductivity and Novel Magnetism*. 2015;28(1):179-190.
25. Tombácz E, Turcu R, Socoliuc V, Vékás L. Magnetic iron oxide nanoparticles: Recent trends in design and synthesis of magnetoresponsive nanosystems. *Biochemical and Biophysical Research Communications*. 2015;468(3):442-453.
26. Salviano LB, Cardoso TMS, Silva GC, Dantas MSS, Ferreira AM. Microstructural Assessment of Magnetite Nanoparticles (Fe_3O_4) Obtained by Chemical Precipitation Under Different Synthesis Conditions. *Materials Research*. 2018;21(2):20170764.
27. Wu S, Sun A, Lu Z, Cheng C, Gao X. Magnetic properties of iron-based soft magnetic composites with SiO_2 coating obtained by reverse microemulsion method. *Journal of Magnetism and Magnetic Materials*. 2015;381:451-456.

28. Ding HL, Zhang YX, Wang S, Xu JM, Xu SC, Li GH. Fe_3O_4@SiO_2 Core/Shell nanoparticles: The Silica Coating Regulations with a Single Core for Different Core Sizes and Shell Thicknesses. *Chemistry of Materials*. 2012;24(23):4572-4580.

29. Tan TTY, Liu S, Zhang Y, Han MY, Selvan ST. Microemulsion Preparative Methods (Overview). In: Andrews DL, Scholes GD, Wiederrecht GP, eds. *Comprehensive Nanoscience and Technology*. Volume 5. London: Elsevier; 2011. p. 339-441.

30. Torres-Luna JA, Carriazo JG. Porous aluminosilicic solids obtained by thermal-acid modification of a commercial kaolinite-type natural clay. *Solid State Sciences*. 2019;88:29-35.

31. Yao X, Zhang L, Li L, Liu L, Cao Y, Dong X, et al. Investigation of the structure, acidity, and catalytic performance of CuO/$Ti_{0.95}Ce_{0.05}O_2$ catalyst for the selective catalytic reduction of NO by NH3 at low temperature. *Applied Catalysis B: Environmental*. 2014;150-151:315-329.

32. Jin Y, Zhao C, Lin Y, Wang D, Chen L, Shen Y. Fe-Based Metal-Organic Framework and its Derivatives for Reversible Lithium Storage. *Journal of Materials Science & Technology*. 2017;33(8):768-774.

33. Komarneni S, Hu W, Noh YD, Van Orden A, Feng S, Wei C, et al. Magnetite syntheses from room temperature to 150 ºC with and without microwaves. *Ceramics International*. 2012;38(3):2563-2568.

34. Cornell RM, Schwertmann U. *The Iron Oxides: Structure, Properties, Reactions, Occurences and Uses*. Weinheim: Wiley-VCH Verlag; 2003.

35. Yang M, Gao L, Liu K, Luo C, Wang Y, Yu L, et al. Characterization of Fe_3O_4/SiO_2/$Gd_2O(CO_3)_2$ core/shell/shell nanoparticles as T1 and T2 dual mode MRI contrast agent. *Talanta*. 2015;131:661-665.

36. Lu AH, Salabas EL, Schüth F. Magnetic Nanoparticles: Synthesis, Protection, Functionalization, and Application. *Angewandte Chemie International Edition*. 2007;46(8):1222-1244.

37. Zhang DE, Zhang XJ, Ni XM, Song JM, Zheng HG. Fabrication and Characterization of Fe_3O_4 Octahedrons via an EDTA-assisted Route. *Crystal Growth & Design*. 2007;7(10):2117-2119.

38. Ristic M, Fujii T, Hashimoto H, Opacak I, Music S. A novel route in the synthesis of magnetite nanoparticles. *Materials Letters*. 2013;100(1):93-97.

39. Harrison RJ, Putnis A. Magnetic properties of the magnetite-spinel solid solution: Curie temperatures, magnetic susceptibilities, and cation ordering. *American Mineralogist*. 1996;81(3-4):375-384.

40. Wu CC, Mason TO. Thermopower Measurement of Cation Distribution in Magnetite. *Journal of the American Ceramic Society*. 1981;64(9):520-522.

41. Levy D, Giustetto R, Hoser A. Structure of magnetite (Fe_3O_4) above the Curie temperature: a cation ordering study. *Physics and Chemistry of Minerals*. 2012;39(2):169-176.

42. Manohar A, Krishnamoorthi C. Low Curie-transition temperature and superparamagnetic nature of Fe_3O_4 nanoparticles prepared by colloidal nanocrystal synthesis. *Materials Chemistry and Physics*. 2017;192:235-243.

43. Brinker CJ, Scherer GW. Sol-Gel Science. *The Physics and Chemistry of Sol-Gel Processing*. San Diego: Academic Press; 1990.

44. Zhang X, Wang J. Preparation of carbon coated Fe_3O_4 nanoparticles for magnetic separation of uranium. *Solid State Sciences*. 2018;75:14-20.

45. Huang F, Li Q, Thorogood GJ, Cheng YB, Caruso RA. Zn-doped TiO_2 electrodes in dye-sensitized solar cells for enhanced photocurrent. *Journal of Materials Chemistry*. 2012;22(33):17128-17132.

46. Ma P, Jiang W, Wang F, Li F, Shen P, Chen M, et al. Synthesis and photocatalytic property of Fe_3O_4@TiO_2 core/shell nanoparticles supported by reduced graphene oxide sheets. *Journal of Alloys and Compounds*. 2013;578:501-506.

47. Costa AL, Ballarin B, Spegni A, Casoli F, Gardini D. Synthesis of nanostructured magnetic photocatalyst by colloidal approach and spray-drying technique. *Journal of Colloid and Interface Science*. 2012;388(1):31-39.

48. Lee J, Lee Y, Youn JK, Na HB, Yu T, Kim H, et al. Simple Synthesis of Functionalized Superparamagnetic Magnetite/Silica Core/Shell Nanoparticles and their Application as Magnetically Separable High-Performance Biocatalysts. *Small*. 2008;4(1):143-152.

49. Liu D, Yuan P, Liu H, Cai J, Qin Z, Tan D, et al. Influence of heating on the solid acidity of montmorillonite: A combined study by DRIFT and Hammett indicators. *Applied Clay Science*. 2011;52(4):358-363.

50. Liu J, Li X, Zhao Q, Ke J, Xiao H, Lv X, et al. Mechanistic investigation of the enhanced NH_3-SCR on cobalt-decorated Ce-Ti mixed oxide: In situ FTIR analysis for structure-activity correlation. *Applied Catalysis B: Environmental*. 2017;200:297-308.

51. Wang L, Li W, Schmieg SJ, Weng D. Role of Brønsted acidity in NH_3 selective catalytic reduction reaction on Cu/SAPO-34 catalysts. *Journal of Catalysis*. 2015;324:98-106.